JACS
JOURNAL OF THE AMERICAN CHEMICAL SOCIETY

Article

pubs.acs.org/JACS

In Situ Solid-State ^{13}C NMR Observation of Pore Mouth Catalysis in Etherification of β-Citronellene with Ethanol on Zeolite Beta

Sambhu Radhakrishnan,[†] Pieter-Jan Goossens,[†] Pieter C. M. M. Magusin,[†,⊥] Sreeprasanth Pulinthanathu Sree,[†] Christophe Detavernier,[‡] Eric Breynaert,[†] Charlotte Martineau,[§,∥] Francis Taulelle,[†,§] and Johan A. Martens*[,†]

[†]Centre for Surface Chemistry and Catalysis, KU Leuven, Celestijnenlaan 200F, Box 2461, 3001 Heverlee, Leuven, Belgium

[§]Tectospin, Institut Lavoisier, UMR 8180, Université de Versailles st. Quentin en Yvelines, 45 Avenue des Etats Unis, 78035 Versailles, Cedex, France

[∥]CEMHTI, CNRS UPR 3079, 1D Avenue de la Recherche Scientifique, 45071 Orléans Cedex 2, France

[‡]Department of Solid State Sciences, CoCooN, Ghent University, Krijgslaan 281 (S1), Ghent 9000, Belgium

Supporting Information

ABSTRACT: The reaction mechanism of etherification of β-citronellene with ethanol in liquid phase over acid zeolite beta is revealed by *in situ* solid-state ^{13}C NMR spectroscopy. Comparison of ^{13}C Hahn-echo and $^{1}H-^{13}C$ cross-polarization NMR characteristics is used to discriminate between molecules freely moving in liquid phase outside the zeolite and molecules adsorbed inside zeolite pores and in pore mouths. In the absence of ethanol, β-citronellene molecules enter zeolite pores and react to isomers. In the presence of ethanol, the concentration of β-citronellene inside zeolite pores is very low because of preferential adsorption of ethanol. The etherification reaction proceeds by adsorption of β-citronellene molecule from the external liquid phase in a pore opening where it reacts with ethanol from inside the pore. By competitive adsorption, ethanol prevents the undesired side reaction of β-citronellene isomerization inside zeolite pores. β-citronellene etherification on zeolite beta is suppressed by bulky base molecules (2,4,6-collidine and 2,6-ditertiarybutylpyridine) that do not enter the zeolite pores confirming the involvement of easily accessible acid sites in pore openings. The use of *in situ* solid-state NMR to probe the transition from intracrystalline catalysis to pore mouth catalysis depending on reaction conditions is demonstrated for the first time. The study further highlights the potential of this NMR approach for investigations of adsorption of multicomponent mixtures in general.

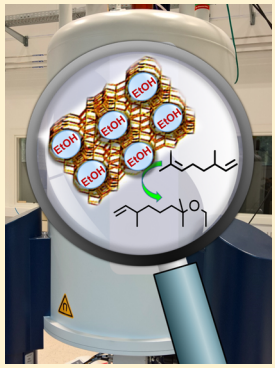

INTRODUCTION

Catalytic processes on zeolites generally involve diffusion and reaction of molecules throughout the intracrystalline pore system.[1] Bulky molecules unable to penetrate the pores can only react in partial cavities and pore openings at zeolite crystal boundaries offering more space than deeper inside the pores.[2] Pore blockage by coke deposition inside the pores can be another reason why the catalytic activity of a zeolite is located at the pore entrances.[3] Pore mouth catalysis accordingly is a particular mechanism for specific combinations of reagent and zeolite. Venuto has been the first to propose pore mouth catalysis in aromatic alkylation.[4] The notion of pore mouth catalysis has been elaborated later on by Fraenkel[5] and Derouane[6] who pointed out that the pockets on the zeolite surface formed by pore termination and cut pore intersections provide a special steric environment for reaction. The peculiar methyl branching selectivity of long *n*-alkanes on medium-pore zeolites such as ZSM-22 has been explained by pore mouth catalysis.[7,8] Long molecules able to span the distance between two neighboring pore openings can penetrate simultaneously with both ends in a separate pore and react according to a key-lock principle.[9,10] In hydrocracking on zeolite Y being a large-pore zeolite, the penetration of heavy alkanes in zeolite crystals seems to be limited to a few nanometers only.[11] Direct experimental evidence for pore mouth catalysis is however difficult to provide. Experimental evidence has been based on adsorption studies,[12] estimation of molecular diffusivity,[13] and molecular and kinetic modeling.[14,15]

Zeolite beta is a prominent catalyst for many applications, and especially for processes related to biomass conversion.[16−22] Sn-beta zeolite catalyst is popular in green chemistry. Examples of catalyzed reactions are conversion of 1,3-dihydroxy acetone to ethyl lactate,[20] isomerization of glucose in aqueous solutions,[21] and Baeyer−Villiger oxidation reactions.[22] Recently we showed acid zeolite beta catalyzes etherification of linear α-olefins and β-citronellene with alcohols.[23−25] In many reactions in the liquid phase, zeolite beta outperforms other zeolites.

NMR is a versatile tool to probe zeolite catalytic chemistry *in situ*.[26−35] There are few if any reports on the use of solid-state NMR for *in situ* investigation of catalysis in mixed phase comprising a liquid reagent in contact with a zeolite. The etherification reaction of β-citronellene with ethanol to ethers proceeds under such reaction conditions at temperatures as low

Received: December 20, 2015
Published: February 4, 2016

DOI: 10.1021/jacs.5b13282
J. Am. Chem. Soc. 2016, 138, 2802−2808

as 80 °C.[23] It is therefore a suitable model reaction for an *in situ* solid-state NMR investigation. Here we use the ^{13}C NMR characteristics in Hahn-echo and $^{1}H-^{13}C$ cross-polarization (CPMAS) spectra to discriminate between molecules freely moving in liquid phase outside the zeolite and adsorbed molecules. From the ensemble of results, we propose an explanation for the exceptional catalytic performances of zeolite beta in a catalytic process in liquid phase.

EXPERIMENTAL SECTION

Ammonium zeolite beta (CP 814C Si/Al = 19) was obtained from Zeolyst. It was converted to the acid form by calcination at 450 °C. Nitrogen adsorption isotherms at −196 °C were determined on a Micromeritics Tristar 3000 instrument. X-ray photoelectron spectra (XPS) were recorded using an S-Probe Monochromatized XPS spectrometer from Surface Science Instruments (VG) with monochromatic Al Kα X-ray (1486.6 eV) source. Binding energy values (BE) were corrected for charging effects by assigning a BE of 284.6 eV to the C 1s signal. Scanning electron microscopy (SEM) was performed on a FEI Nova NanoSEM450 (FEI) instrument at 2 kV. FTIR spectra were recorded on a Nicolet 6700 spectrometer. A pressed self-supporting zeolite wafer weighing ca. 20 mg was mounted in a vacuum cell inside the spectrometer. The sample was evacuated at 400 °C for 1 h. Adsorption of pyridine and 2,4,6-collidine was performed by exposing the pellet to vapor of the compound (ca. 4−5 kPa) at 150 °C for 10 min. Desorption was done by raising the temperature. Spectra were recorded at 200 and 400 °C. The molar extinction coefficient for Brønsted and Lewis acid site quantification using pyridine was taken from Emeis[36] and for adsorbed 2,4,6-collidinium ion from Nesterenko et al.[37]

(+)-β-citronellene (99%) used in the NMR studies was obtained from Sigma-Aldrich, and absolute ethanol was from VWR. For *in situ* solid-state NMR spectroscopy acid zeolite beta powder was dried under N_2 flow at 400 °C for 3 h. Dry zeolite powder was combined with β-citronellene or β-citronellene−ethanol mixture (1:10 molar ratio) in proportions of 0.6 mL/g to obtain a wet powder. Contact with the ambient was avoided to prevent uptake of air-borne water vapor. *In situ* MAS NMR experiments were performed on a Bruker Ascend 500 MHz spectrometer (static magnetic field of 11.7 T) with 4 mm H/X/Y MAS probe at room temperature with a rotor spinning rate of 5 kHz. ^{13}C NMR signal was monitored via two methods: direct excitation with Hahn-echo acquisition[38] and cross-polarization (CP).[39,40] For Hahn-echo pulse sequence, a delay of 400 μs, two rotor periods, between 90° and 180° pulses, 4.5 μs 90° pulse length, recycle delay of 3 s, 4096 scans, and ^{1}H SPINAL-64[41] decoupling (70 kHz) during signal acquisition were used. The $^{1}H-^{13}C$ CPMAS NMR spectra were recorded using 50 kHz RF field on ^{13}C, a RAMPed pulse on ^{1}H (100−80%) for the contact, 4096 scans, recycle delay of 3 s, ^{1}H SPINAL-64 decoupling,[41] and a contact time of 5 ms. Both experiments took ca. 3.5 h. The ^{13}C chemical shifts are referenced to TMS.

Catalytic etherification experiments were performed in a liquid phase, continuous flow, tubular reactor with internal free diameter of 9 mm. The catalyst bed consisted of 1.5 g of compressed zeolite beta particles (diameter range of 250−500 μm). A layer of quartz spheres (2 mm diameter) was positioned upstream for preventing channeling of the liquid flow. The catalyst was pretreated at 200 °C under N_2 gas flow (100 mL/min) for 2 h followed by calcination at 450 °C under O_2 flow (150 mL/min) for 2 h. *n*-Heptane (>99%) and 2,4,6-collidine (>99%) were from Acros Organics, and 2,6-ditertiarybutylpyridine (>97%) and β-citronellene (ca. 91% β-citronellene, ca. 7% 1-isopropenyl-2,3-dimethyl-cyclopentane and ca. 2% 1-methyl-4-(propan-2-ylidene)cyclohexane isomers) were from Sigma-Aldrich. *n*-Heptane was verified to be inert under reaction conditions and was used as internal standard. In catalyst poisoning experiments, 1 wt % 2,4,6-collidine or 2,6-ditertiary butylpyridine was added to the feed mixture of β-citronellene and ethanol. For GC analysis of reactions products using FID detector, response factors of identified reaction products were calculated by effective carbon number method.[42]

RESULTS AND DISCUSSION

The investigated zeolite beta sample is a spherical aggregate of crystallites measuring 20−60 nm (Figure 1). The BET specific

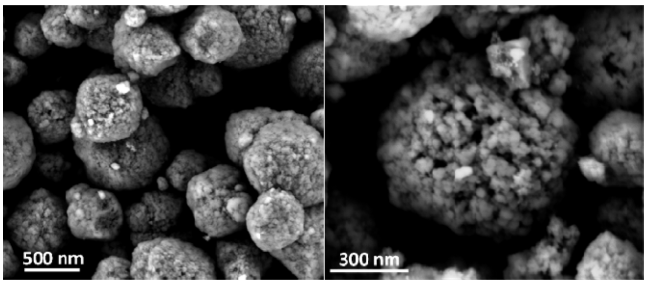

Figure 1. Scanning electron micrographs of zeolite beta sample at two magnifications.

surface area is ca. 486 m^2/g, and the micropore volume is ca. 0.23 cm^3/g, typical of zeolite beta.[43] The presence of compositional gradients was probed by determining the Si/Al ratio at the external surface using XPS and comparison with overall composition. The Si/Al atomic ratio of 17 at the external surface was similar to the overall Si/Al ratio of 19 revealing absence of significant compositional gradients.

Quantification of Brønsted and Lewis type acid sites was done by titration with pyridine and FTIR spectroscopy. The pyridine molecule with kinetic diameter of 0.59 nm has access to zeolite beta pores having a minimum free diameter of ca. 0.67 nm.[44] Pyridine adsorbed on Brønsted and Lewis acid sites generates characteristic IR absorption bands at 1540 and 1450 cm^{-1}, respectively.[36,45] Brønsted acid sites are due to protons compensating negative framework charge deficits caused by trivalent aluminum incorporation in tetrahedral framework. Lewis acid sites are typically due to extra-framework Al species. Zeolite beta has Brønsted acid sites mainly, and only low amounts of Lewis acid sites (Table 1). Pyridine adsorption at

Table 1. Acidity of Zeolite Beta

total acid sites[a] (mmol/g)	Brønsted	0.516
	Lewis	0.166
strong acid sites[b] (mmol/g)	Brønsted	0.230
	Lewis	0.094
total pore mouth sites[c] (mmol/g)	Brønsted	0.117
strong pore mouth sites[d] (mmol/g)	Brønsted	0.078
accessibility index (ACI)[e]	Brønsted	0.23

[a]Pyridine adsorption at 200 °C. [b]Pyridine adsorption at 400 °C. [c]2,4,6-Collidine adsorption at 200 °C. [d]2,4,6-Collidine adsorption at 400 °C. [e]Molar ratio of acid sites accessible to 2,4,6-collidine to acid sites probed by pyridine at 200 °C.

200 °C was considered to probe all acid sites. At 400 °C, pyridine probes strong acid sites. A significant share of the Brønsted acid sites are strong (Table 1). Polymethyl-substituted pyridine bases like 2,4,6-collidine (kinetic diameter 0.74 nm)[37,45] can be used for quantification of acid sites with less steric constraint than inside the pores. Thibault-Starzyk et al. proposed the accessibility index (ACI) as the ratio of the number of acid sites detected by adsorption of the probe to the total amount of acid sites in the zeolite, to quantify the share of acid sites with enhanced accessibility.[45] For large pore zeolites like beta, all the acid sites will be accessible to pyridine, and hence the ACI could be calculated as the ratio of the amount of

DOI: 10.1021/jacs.5b13282
J. Am. Chem. Soc. 2016, 138, 2802−2808

acid sites accessible to bulky probe (2,4,6-collidine) to the amount of acid sites probed by pyridine.[45] The ACI of zeolite beta, determined using 2,4,6-collidine and pyridine for probing, respectively, Brønsted acid sites at pore mouths and in total, was 0.23. Zeolite beta has a three-dimensional (3D) pore system with intersecting channels in the three directions[44] such that all crystal facets have pore openings. Based on the ACI value, the zeolite beta crystal structure, and assuming uniform acid site concentration (absence of compositional gradients evidenced by XPS, vide supra), the penetration depth of 2,4,6-collidine into the zeolite crystallites measuring 40 nm on average was estimated at ca. 2.5 nm. This penetration depth is about thrice the molecular size of 2,4,6-collidine. Despite the roughness of this estimation of penetration depth, it shows 2,4,6-collidine selectively probes acid sites at very limited depth. The ACI of zeolite beta is higher than for medium-pore zeolites like H-ZSM-5 (ACI = 0.06)[45] and large-pore mordenite zeolite (ACI = 0.18).[37] The small particle size (Figure 1) and the tridimensional pore system with pore openings on all crystal facets explain the high ACI value.

NMR investigations were performed using commercially available enantiopure (+)-β-citronellene liquid. Since enantioselectivity is beyond the scope of the present study, the compound further on is denoted simply as β-citronellene. NMR chemical shifts of ^{13}C nuclei in β-citronellene, ethanol, the preferred etherification product (7-ethoxy-3,7-dimethyloct-1-ene), and the hydration product 2,6-dimethyl-oct-7-en-2-ol were assigned via a combination of 1D and 2D liquid-state NMR experiments (Figure 2).

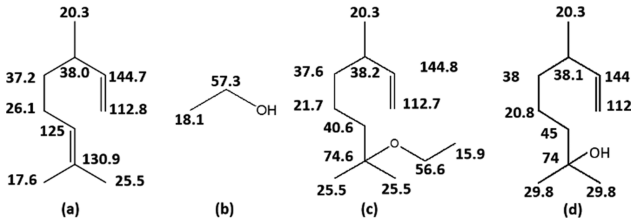

Figure 2. Experimentally assigned ^{13}C NMR chemical shifts (ppm) of (a) (+)-β-citronellene, (b) ethanol, (c) β-citronellyl ether -7-ethoxy-3,7-dimethyloct-1-ene, and (d) hydration product -2,6-dimethyl-oct-7-en-2-ol.

For this study, we rely on differences of relaxation properties of molecules inside and outside zeolite pores. Outside molecules are expected to be very mobile, liquid-like, leading to narrow NMR resonances and reduced ^{1}H−^{13}C residual dipolar couplings with very inefficient CP transfer and longitudinal relaxation times (T_1) shorter than in the solid-state.[46] On the contrary, molecules inside zeolite pores are expected to have reduced mobility and the possibility to adopt several conformations. This results in heterogeneous broadening of the ^{13}C NMR resonances. NMR resonances for each chemically identical function will be distributed according to the different conformations, each contributing a narrow component to the observed broad signal. ^{1}H−^{13}C residual dipolar coupling in adsorbed state is favorable for polarization transfer. Therefore, direct acquisition of ^{13}C NMR spectra through a Hahn-echo sequence allows observation of both mobile molecules (narrow lines) and adsorbed molecules (broad signals), while ^{1}H−^{13}C CPMAS NMR spectra allow for selective observation of the adsorbed molecules. Line width reflects the degree of conformation distribution.

To gain insight in adsorption and reaction of β-citronellene on zeolite beta, three different samples were investigated (Table 2). In experiment 1, dehydrated zeolite beta was contacted with

Table 2. Molar Proportions of Species in Samples Investigated in NMR Experiments

zeolite + adsorbate	amount of acid sites[a] (mmol/g)	β-citronellene (mmol/g)	water (mmol/g)	ethanol (mmol/g)
beta dry + β-citronellene	0.516	3.34	0	0
beta wet + β-citronellene	0.516	3.34	6.1	0
beta dry + β-citronellene + ethanol	0.516	0.834	0	8.34

[a]Measured by pyridine adsorption.

β-citronellene liquid. Experiment 2 was similar except zeolite beta was hydrated. In Experiment 3, dehydrated zeolite beta was contacted with a mixture of ethanol and β-citronellene.

Experiment 1. Liquid β-citronellene and dehydrated zeolite beta were mixed in a proportion of 0.6 mL/g. The added liquid volume of β-citronellene exceeded the zeolite micropore volume (0.23 mL/g). The ^{13}C Hahn-echo NMR spectrum (Figure 3b red) exhibits the expected resonances of β-citronellene next to resonances because isomers of the β-citronellene molecule formed catalytically during the NMR experiment (4 h). The assignment of these resonances to individual isomers is provided in Supporting Information (S4). As mentioned above, direct acquisition of the ^{13}C NMR spectrum through a Hahn-echo pulse sequence reveals resonances of mobile and adsorbed species. A broad underlying resonance extending from ca. 10 to 50 ppm can be observed. It is ascribed to aliphatic C atoms of β-citronellene molecules (Figure 2) and the different isomers (Supporting Information S4), all with limited mobility, i.e., adsorbed in the zeolite pores. The narrow resonances of olefinic C atoms of β-citronellene and its isomers with their different chemical shifts were assigned (Figure 2 and Supporting Information S4). In the ^{13}C CPMAS NMR spectrum (Figure 3b black), only the rigid molecules are observed. This spectrum corresponds to the broad resonances that were observed on the Hahn-echo spectrum, which confirms the assignment to adsorbed molecules. These ^{13}C resonances are very broad, reflecting the variety of conformations of β-citronellene and its isomers inside zeolite pores. Finally, narrow resonances of reagent and product molecules indicate that a fraction of the remaining β-citronellene and products are in liquid state, outside the zeolite. NMR experiment 1 confirms the penetration and reaction of β-citronellene in the zeolite pores at room temperature.

Experiment 2. A sample of zeolite beta containing adsorbed moisture from ambient air (0.11 mL/g) was combined with liquid β-citronellene (0.6 mL/g) and filled in the NMR rotor. The ^{13}C Hahn-echo NMR spectrum (Figure 3c red) displays essentially narrow resonances, which reveal the presence of β-citronellene molecules in the mobile state, i.e., outside the pores. The ^{13}C CPMAS spectrum (Figure 3c gray) visualized the signature of 2,6-dimethyl-oct-7-en-2-ol characterized by resonances at ca. 75 and ca. 41 ppm. This reaction product is formed via hydration of the β double bond of β-citronellene. The two resonances at 113 and 145 ppm are assigned to the β-citronellene and α-double bond of the β-

DOI: 10.1021/jacs.5b13282
J. Am. Chem. Soc. 2016, 138, 2802−2808

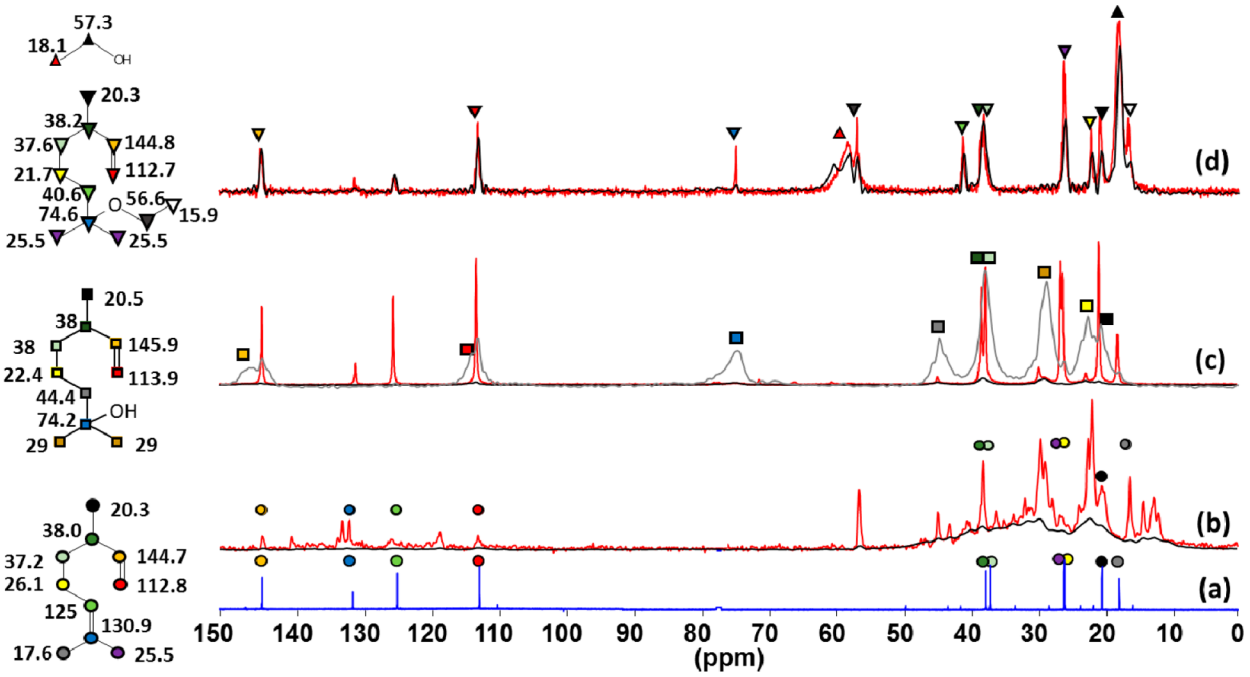

Figure 3. $^{13}C\{^{1}H\}$ solid-state MAS NMR spectra acquired with a Hahn-echo (in red) and CP (in black): (a) ^{13}C liquid-state NMR spectrum; (b) dehydrated zeolite beta mixed with β-citronellene (experiment 1); (c) hydrated zeolite beta mixed with β-citronellene (Experiment 2); CP spectrum magnified for clarity (in gray); and (d) dehydrated zeolite beta mixed with β-citronellene and ethanol (molar ratio of 1:10); number of scans = 4096 (b–d).

olefin hydration product (Figure 2). The limited line width of resonances of the CPMAS spectrum of the sample with hydrated zeolite beta (Figure 3c black) compared to dehydrated zeolite (Figure 3b black) is due to the uniqueness of the product formed. Comparison of the NMR data of β-citronellene adsorbed on dehydrated and hydrated zeolite beta (Figures 3b and c) therefore shows that the water molecules in the zeolite pores strongly compete with β-citronellene for adsorption.

Experiment 3. The etherification reaction was performed by contacting dehydrated zeolite beta with a mixture of β-citronellene and ethanol. In the ^{13}C Hahn-echo NMR spectrum, β-citronellene C atoms appear as narrow resonances, while ethanol carbon atoms give rise to broadened ^{13}C resonances at 57 and 18 ppm (Figure 3d red). Ethanol is adsorbed in the zeolite pores with limited mobility, while the β-citronellene molecules exhibiting narrow signals exhibit a large degree of freedom like in liquid state. In the ^{13}C CPMAS NMR spectrum (Figure 3d black), ethanol molecules remain characterized by broad peaks, but β-citronellene shows up with narrow resonances, as narrow as in the Hahn-echo spectrum. This last feature in CPMAS is ascribed to β-citronellene molecules in adsorbed state enabling residual dipolar coupling and polarization transfer, while at the same time retaining a high degree of conformational freedom. This proves that the β-citronellene molecules are adsorbed at sites enabling mobility, which can be the pore entrances. It is difficult to envision another location in the sample which can provide such NMR characteristics. Citronellyl ether formation is indicated by the emergence of ^{13}C resonances at 74.6, 56.6, and 40.6 ppm (Figure 2). The earlier observed etherification selectivity at the β-double bond compared to the α-double bond in β-citronellene[23] is confirmed by the gradual disappearance of the ^{13}C resonances of the β-double bond carbons (125 and 130.9 ppm, Figure 2), while resonances of α-double bond carbons (112.7 and ca. 144.8 ppm) are unaffected (Figure 4). The NMR resonances of the citronellyl ether exhibit narrow line widths in the CPMAS spectrum, similar to β-citronellene. The ether product visualized with CPMAS resides on the same location as the reagent, i.e., on pore mouths. This location of the molecules according to the NMR experiments offers insight into the reaction mechanism and explains the selective reaction. The occupation of the pores with ethanol forces β-citronellene molecules to react with ethanol at pore openings on the external surface. Isomerization reaction requiring penetration of β-citronellene deeper into the pores is suppressed. The high activity of zeolite beta in the

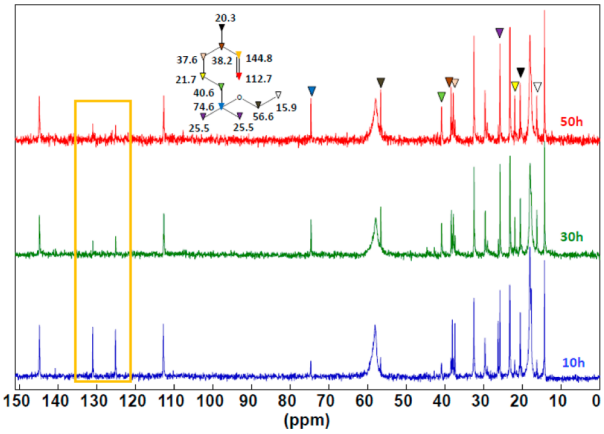

Figure 4. Time evolution of $^{13}C\{^{1}H\}$ solid-state MAS NMR Hahn-echo spectrum of zeolite beta contacted with mixture of β-citronellene and ethanol (molar ratio of 1:10) and 17 wt % *n*-heptane as internal standard. Resonances assigned to citronellyl ether are indicated. The yellow frame highlights the disappearance of resonances of the β-double bond of β-citronellene with time.

DOI: 10.1021/jacs.5b13282
J. Am. Chem. Soc. 2016, 138, 2802–2808

etherification reaction is due to its 3D pore system and small crystallite size (Figure 1), offering plenty of readily available acid sites at pore mouths according to the high ACI value of 0.23 (Table 1). A possible reaction mechanism of etherification is presented in Scheme 1. The high selectivity for etherification

Scheme 1. Proposed Reaction Scheme of β-Citronellene Etherification with Ethanol on Pore Mouth Acid Sites of Zeolite Beta

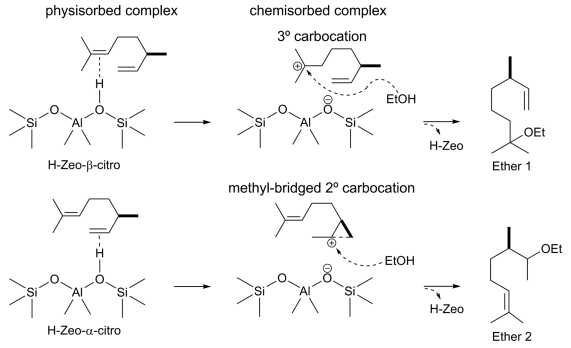

at the β-double bond suggests the reaction proceeds by protonation of β-citronellene rather than ethanol. Etherification at the β-double bond is kinetically favored because of formation of a tertiary alkylcarbenium ion reaction intermediate on β-double bond protonation, which is more stable than the secondary alkylcarbenium ion intermediate formed upon protonation at the α-double bond.[23] The stability of the alkylcarbenium ion can be critical when reaction occurs on weaker acid sites in pore mouths and in competitive adsorption with ethanol. Isomerization (and oligomerization leading to coke formation observed in kinetic experiments at 80−120 °C)[23] involving both α- and β-double bonds of β-citronellene (Supporting Information) catalyzed by acid sites deeper inside the zeolite pores is suppressed by the limited access of the molecule to the pores.

Many reactions catalyzed by zeolite beta involve water and/or alcohols.[16−22] Competitive adsorption in favor of water and alcohol observed in this study offers an explanation why zeolite beta performs well in many types of liquid-phase catalysis.

Selective poisoning of pore mouth acid sites using bulky base molecules that do not enter the channels of the zeolite can be used to probe pore mouth catalysis *in situ* in a reactor. Du et al. used 2,4,6-collidine poisoning to demonstrate the role played by easily accessible acid sites in benzene alkylation with ethylene over acid MCM-22 zeolite.[47] Kim et al. used selective poisoning with triphenyl phosphine oxide to investigate the influence of external surface acid sites of MFI nanosheets in catalytic cracking of triisopropylbenzene.[48]

β-citronellene etherification was performed on zeolite beta catalyst in a fixed bed continuous flow liquid-phase reactor using a feed mixture with a molar ratio of β-citronellene:EtOH of 1:10 at a pressure of 6 MPa. At a reaction temperature of 80 °C, β-citronellene conversion reached ca. 50% with a selectivity to the ether of ca. 80%, and ca. 90% chemoselectivity for etherification at the β-double bond as compared to the α-double bond was achieved (Figure 5a). Addition of 1 wt % 2,4,6-collidine to the feed caused the activity of zeolite beta catalyst to decrease with increasing time on stream until 6 h, after which the catalyst was entirely poisoned (Figure 5a). The attenuation of catalytic activity by 2,4,6-collidine, a base

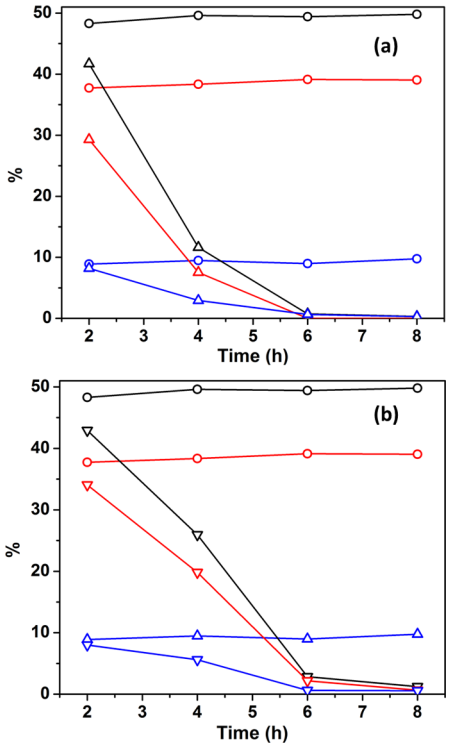

Figure 5. Time evolution of conversion (black trace), etherification yield (red trace), and isomer yield (blue trace) in β-citronellene etherification reaction with ethanol over H-beta zeolite (circle), 2,4,6-collidine poisoned H-beta zeolite (triangle, a), and 2,6-ditertiarybutylpyridine poisoned H-beta zeolite (inverted triangle, b). Reaction conditions: T = 80 °C; feed: 1:10 β-citronellene:EtOH (mol: mol), 17 wt % *n*-heptane, and with/without ca. 1 wt % 2,4,6-collidine or 2,6-ditertiarybutylpyridine; WHSV = 3.8 h^{-1}.

molecule unable to penetrate the pores, confirms that the catalytic sites for etherification are indeed located at the pore mouths. A similar poisoning experiment using 2,6-ditertiary butylpyridine (kinetic diameter > 1.05 nm)[49,50] showed a similar deactivation pattern (Figure 5b). Parvulescu et al. investigated spent zeolite beta catalysts for etherification reactions of long linear olefins with alcohols like glycols and glycerol using confocal fluorescence spectroscopy.[51] Based on the distribution of coke products on the zeolite crystals, they concluded that activity is concentrated at the rim of the crystals, like in this study.[51]

CONCLUSIONS

The reaction mechanism of etherification of β-citronellene with ethanol in liquid phase on zeolite beta is revealed using *in situ* ^{13}C Hahn-echo and CPMAS NMR spectroscopy. Undesired isomerization reactions of β-citronellene can be suppressed by preventing the molecule from penetrating the pores of the zeolite. This is achieved in the presence of excess ethanol being preferentially adsorbed in the zeolite pores. The etherification reaction proceeds at easily accessible acid sites in pore openings. The β-double bond of β-citronellene preferentially is protonated by acid sites at such location leading to selective etherification reaction with ethanol molecule provided from inside the pores. Catalysis occurring at pore mouths is supported by the observed activity attenuation on selective acid site poisoning with bulky base molecules. Zeolite beta with its small crystal size (20−60 nm) is uniquely suited for liquid-

DOI: 10.1021/jacs.5b13282
J. Am. Chem. Soc. 2016, 138, 2802−2808

phase catalysis involving small molecules such as alcohols and water preventing penetration of larger organic reagents deep in the pores where they can undergo undesired side reactions and give rise to coke formation and deactivation. The here presented NMR approaches are also applicable to probe selective adsorption on zeolite in contact with multicomponent liquid.

■ ASSOCIATED CONTENT

Supporting Information

The Supporting Information is available free of charge on the ACS Publications website at DOI: 10.1021/jacs.5b13282.

In situ FT-IR investigation of pore mouth blocking on 2,4,6-collidine adsorption; equations for calculation of conversion and selectivity in catalytic reactions; signal assignment of β-citronellene and citronellyl ethers using liquid-state NMR spectroscopy; identification of β-citronellene isomers formed *in situ* on impregnation of dry beta zeolite with β-citronellene; N_2 sorption isotherm; FT-IR spectra of pyridine adsorbed on zeolite beta; FT-IR spectra of 2,4,6-collidine adsorbed on zeolite beta; 2,4,6-collidine penetration estimation (PDF)

■ AUTHOR INFORMATION

Corresponding Author

*Johan.Martens@biw.kuleuven.be

Present Address

⊥The Grey group, Department of Chemistry, University of Cambridge, Lensfield Road, Cambridge, CB2 1EW, United Kingdom.

Notes

The authors declare no competing financial interest.

■ ACKNOWLEDGMENTS

J.A.M. acknowledges the Flemish Government for long-term structural funding (Methusalem) and the Belgian government for interuniversity attraction poles (IAP). This work was supported by the Flemish FWO. C.D. acknowledges FWO–Vlanderen, BOF-UGent (GOA 01G01513) and the Hercules Foundation (AUGE/09/014) for funding. The authors acknowledge Karel Deurinckx for liquid-state NMR measurements.

■ REFERENCES

(1) *Zeolites and Catalysis: Synthesis, Reactions and Applications*; Cejka, J., Corma, A., Zones, S., Eds.; Wiley VCH: Weinheim, 2010.

(2) Martens, J. A.; Jacobs, P. A. Some Aspects of Molecular Shape Selective Catalysis with Hydrocarbons in Zeolites. In *Zeolite Microporous Solids: Synthesis, Structure, and Reactivity*, NATO ASI Series; Derouane, E. G., Lemos, F., Naccache, C., Ribeiro, F. R., Eds.; Springer: Dordrecht, The Netherlands, 1992; Vol. 352, pp 511–529.

(3) *Deactivation and Regeneration of Zeolite Catalysts - Catalytic Science Series*; Guisnet, M., Ribeiro, F. R., Eds.; Imperial College Press: London, 2011; Vol. 9.

(4) Venuto, P. B. Aromatic Reactions over Molecular Sieve Catalysts: A Mechanistic Review. In *Catalysis in Organic Syntheses 1977*; Gerard, Smith, Ed.; Academic Press, New York, 1977; pp: 67–93.

(5) Fraenkel, D.; Cherniavsky, M.; Ittah, B.; Levy, M. *J. Catal.* **1986**, *101*, 273.

(6) Derouane, E. G.; Andre, J.-M.; Lucas, A. A. *J. Catal.* **1988**, *110*, 58.

(7) Martens, J. A.; Vanbutsele, G.; Jacobs, P. A.; Denayer, J.; Ocakoglu, R.; Baron, G.; Muñoz Arroyo, J. A.; Thybaut, J.; Marin, G. B. *Catal. Today* **2001**, *65*, 111.

(8) Claude, M. C.; Martens, J. A. *J. Catal.* **2000**, *190*, 39.

(9) Martens, J. A.; Verboekend, D.; Thomas, K.; Vanbutsele, G.; Pérez-Ramírez, J.; Gilson, J.-P. *Catal. Today* **2013**, *218–219*, 135.

(10) Martens, J. A.; Souverijns, W.; Verrelst, W.; Parton, R.; Froment, G. F.; Jacobs, P. A. *Angew. Chem., Int. Ed. Engl.* **1995**, *34*, 2528.

(11) Zecevic, J.; Vanbutsele, G.; de Jong, K. P.; Martens, J. A. *Nature* **2015**, *528*, 245.

(12) Ocakoglu, R. A.; Denayer, J. F. M.; Marin, G. B.; Martens, J. A.; Baron, G. V. *J. Phys. Chem. B* **2003**, *107*, 398.

(13) Katzer, J. R., Ph. D. Thesis, Massachusetts Institute of Technology, Cambridge, MA, 1969.

(14) Laxmi Narasimhan, C. S.; Thybaut, J. W.; Marin, G. B.; Jacobs, P. A.; Martens, J. A.; Denayer, J. F.; Baron, G. V. *J. Catal.* **2003**, *220*, 399.

(15) Laxmi Narasimhan, C. S.; Thybaut, J. W.; Marin, G. B.; Denayer, J. F.; Baron, G. V.; Martens, J. A.; Jacobs, P. A. *Chem. Eng. Sci.* **2004**, *59*, 4765.

(16) Goodwin, J. G.; Natesakhawat, S.; Nikolopoulos, A. A.; Kim, S. Y. *Catal. Rev.: Sci. Eng.* **2002**, *44*, 287.

(17) Jansen, J. C.; Creyghton, E. J.; Njo, S. L.; van Koningsveld, H.; van Bekkum, H. *Catal. Today* **1997**, *38*, 205.

(18) Mukarakate, C.; Watson, M. J.; ten Dam, J.; Baucherel, X.; Budhi, S.; Yung, M. M.; Ben, H.; Iisa, K.; Baldwin, R. M.; Nimlos, M. R. *Green Chem.* **2014**, *16*, 4891.

(19) Aho, A.; Kumar, N.; Eränen, K.; Salmi, T.; Hupa, M.; Murzin, D. Y. *Process Saf. Environ. Prot.* **2007**, *85*, 473.

(20) Dijkmans, J.; Dusselier, M.; Gabriëls, D.; Houthoofd, K.; Magusin, P. C. M. M.; Huang, S.; Pontikes, Y.; Trekels, M.; Vantomme, A.; Giebeler, L.; Oswald, S.; Sels, B. F. *ACS Catal.* **2015**, *5*, 928.

(21) Moliner, M.; Roman-Leshkov, Y.; Davis, M. E. *Proc. Natl. Acad. Sci. U. S. A.* **2010**, *107*, 6164.

(22) Corma, A.; Nemeth, L. T.; Renz, M.; Valencia, S. *Nature* **2001**, *412*, 423.

(23) Radhakrishnan, S.; Purino, M.; Alexopoulos, K.; Taulelle, F.; Reyniers, M.-F.; Marin, G. B.; Martens, J. A. *Green Chem.* **2015**, *17*, 2840.

(24) Radhakrishnan, S.; Franken, J.; Martens, J. A. *Green Chem.* **2012**, *14*, 1475.

(25) Radhakrishnan, S.; Thoelen, G.; Franken, J.; Degrève, J.; Kirschhock, C. E. A.; Martens, J. A. *ChemCatChem* **2013**, *5*, 576.

(26) Ivanova, I. I.; Kolyagin, Y. G. *Chem. Soc. Rev.* **2010**, *39*, 5018.

(27) Haw, J. F.; Song, W.; Marcus, D. M.; Nicholas, J. B. *Acc. Chem. Res.* **2003**, *36*, 317.

(28) Wang, W.; Jiang, Y.; Hunger, M. *Catal. Today* **2006**, *113*, 102.

(29) Haouas, M.; Walspurger, S.; Taulelle, F.; Sommer, J. *J. Am. Chem. Soc.* **2004**, *126*, 599.

(30) Wolf, P.; Valla, M.; Rossini, A. J.; Comas-Vives, A.; Núñez-Zarur, F.; Malaman, B.; Lesage, A.; Emsley, L.; Copéret, C.; Hermans, I. *Angew. Chem., Int. Ed.* **2014**, *53*, 10179.

(31) Borghèse, S.; Haouas, M.; Sommer, J.; Taulelle, F. *J. Catal.* **2013**, *305*, 130.

(32) Haouas, M.; Fink, G.; Taulelle, F.; Sommer, J. *Chem. - Eur. J.* **2010**, *16*, 9034.

(33) Arzumanov, S. S.; Reshetnikov, S. I.; Stepanov, A. G.; Parmon, V. N.; Freude, D. *J. Phys. Chem. B* **2005**, *109*, 19748.

(34) Stepanov, A. G.; Sidelnikov, V. N.; Zamaraev, K. I. *Chem. - Eur. J.* **1996**, *2*, 157.

(35) Gabrienko, A. A.; Arzumanov, S. S.; Luzgin, M. V.; Stepanov, A. G.; Parmon, V. N. *J. Phys. Chem. C* **2015**, *119*, 24910.

(36) Emeis, C. A. *J. Catal.* **1993**, *141*, 347.

(37) Nesterenko, N. S.; Thibault-Starzyk, F.; Montouillout, V.; Yushchenko, V. V.; Fernandez, C.; Gilson, J.-P.; Fajula, F.; Ivanova, I. I. *Kinet. Catal.* **2006**, *47*, 40.

(38) Hahn, E. *Phys. Rev.* **1950**, *80*, 580–594.

DOI: 10.1021/jacs.5b13282
J. Am. Chem. Soc. 2016, 138, 2802–2808

(39) Pines, A.; Gibby, M. G.; Waugh, J. S. *Chem. Phys. Lett.* **1972**, *15*, 373−376.
(40) Hartmann, S.; Hahn, E. *Phys. Rev.* **1962**, *128*, 2042−2053.
(41) Fung, B.; Khitrin, A.; Ermolaev, K. *J. Magn. Reson.* **2000**, *142*, 97−101.
(42) Dietz, W. A. *J. Chromatogr. Sci.* **1967**, *5*, 68.
(43) Nanda, M. R.; Yuan, Z.; Qin, W.; Ghaziaskar, H. S.; Poirier, M.-A.; Xu, C. *Appl. Energy* **2014**, *123*, 75.
(44) International Zeolite Association. *Database of Zeolite Structures - Framework Type *BEA*; http://izasc.biw.kuleuven.be/fmi/xsl/IZA-SC/ftc_fw.xsl?-db=Atlas_main&-lay=fw&-max=25&STC=BEA&-find (accessed January 29, 2016).
(45) Thibault-Starzyk, F.; Stan, I.; Abelló, S.; Bonilla, A.; Thomas, K.; Fernandez, C.; Gilson, J.-P.; Pérez-Ramírez, J. *J. Catal.* **2009**, *264*, 11.
(46) Kerkhofs, S.; Saïdi, F.; Vandervoort, N.; Van den Mooter, G.; Martineau, C.; Taulelle, F.; Martens, J. A. *J. Mater. Chem. B* **2015**, *3*, 3054.
(47) Du, H.; Olson, D. H. *J. Phys. Chem. B* **2002**, *106*, 395.
(48) Kim, W.; Ryoo, R. *Catal. Lett.* **2014**, *144*, 1164.
(49) Góra-Marek, K.; Tarach, K.; Choi, M. *J. Phys. Chem. C* **2014**, *118*, 12266.
(50) Fărcaşiu, D.; Leu, R.; Corma, A. *J. Phys. Chem. B* **2002**, *106*, 928.
(51) Parvulescu, A. N.; Mores, D.; Stavitski, E.; Teodorescu, C. M.; Bruijnincx, P. C. A.; Gebbink, R. J. M. K.; Weckhuysen, B. M. *J. Am. Chem. Soc.* **2010**, *132*, 10429.

DOI: 10.1021/jacs.5b13282
J. Am. Chem. Soc. 2016, 138, 2802−2808